Analysis of the effect of probe structure on sampling accuracy in supersonic airflow

Yingtao Chen [1, a], Wanlin Zhang [1, b], Pengpeng Sha [2, c], and Xinlong Yang [1, d]

[1] School of Aero Engine, Shenyang Aerospace University, Shenyang 110136, China;

[2] AECC Sichuan Gas Turbine Establishment, Mianyang Sichuan 621000, China.

[a] Chenyingtao75@163.com, [b] 15242339718@163.com, [c] 541600179@qq.com,

[d] 2397108920@163.com

Abstract. The accuracy of the sampling of the gas components has a significant impact on the measurement of various performance parameters in the combustion chamber of an aero-engine. This paper examines the accuracy of a six-point gas sampling probe when used in supersonic airflow. A numerical simulation method of component transport and fluid-solid coupling is employed to construct a three-dimensional probe multi-component gas flow characteristic solution model. Three kinds of probes with 28°, 30° and 32° angles and structure-modified conical probes were established, and the influence law of probe structure on gas sampling accuracy was analyzed. The results of the study demonstrate that the 28° and structurally modified conical probes yield a more effective improvement in sampling accuracy in comparison to the original 30° structure. The test data of the test bench are in good agreement with the simulation results, thereby demonstrating the reliability and accuracy of the sampling probe following structural modification.

Keywords: supersonic airflow; sampling probe; sampling accuracy; numerical simulation.

1. Introduction

Gas analysis involves gathering high enthalpy gas via the sampling system. This is a crucial method of appraising engine performance [1-3]. One reliable and cost-effective way of extracting gas is by using the probe sampling method, which involves capturing samples from the combustion chamber using a sampling probe [4]. To ensure the authenticity and representativeness of the results, it is crucial to maintain gas composition consistency before and during sampling. In the 1960s, foreign researchers Williamson et al. [5] pioneered the use of gas analysis in jet engine combustion temperature research. In the 1980s, the National Aeronautics and Space Administration (NASA) established a computational procedure to derive the performance of combustion chambers using gas component parameters. This gas analysis method has thus entered the ranks of conventional measurement techniques [6]. In 2010, Sevcenco et al. [7] constructed a gas analysis system with the objective of evaluating the real-time size and volume of gas turbine exhaust. Mutschler et al. [8] subsequently improved the traditional gas chromatography gas analysis method, enabling the analysis of reaction kinetics. In 2016, the American Society of Motor Vehicle Engineers developed a continuous sampling of gas emissions from aerospace gas turbine engines based on the gas analysis method. The method of emission measurement procedure [9-10] enables continuous sampling and analysis of gas emissions from gas turbine engines.

Owing to the probe's short internal flow path, gas rapidly passes through it. Typically, the probe head employs an expansion channel and an external water-cooling system to cool the sample gas to a point where no chemical reaction occurs. [7-8]. The precision of extracting gas components in gas analysis significantly affects the measurement of different performance parameters of the engine combustion chamber. Moreover, the detached shock wave produced by the probe head under the supersonic airflow drastically influences the head incoming flow, leading to the deviation of the concentration and volume fraction of each gas component. Previous research has not adequately investigated the impact of flow parameters on the accuracy error of gas components, this study therefore develops a flow characteristic model for a sampling probe and uses numerical simulations to analyze the supersonic gas flow sampling process. The study analyzes the internal and external

flow characteristics, as well as the sampling accuracy of probes with angles of 28°, 30° and 32°. An optimal probe design is then developed to calculate combustion efficiency errors during various working conditions, which can provide optimal sampling conditions for actual testing.

2. Solving Model and Computational Methods

2.1 Solving model

In this study, a six-point gas sampling probe is used as the fundamental research model. The structure of the probe and the internal flow channels are shown in Figure 1, where the shape of the detached shock wave that can be generated at the probe head from supersonic speeds is labelled. The probe comprises a protective casing, a probe, six groups of gas conduits, and a water-cooling system. The dimensions of the flow channel inside the probe are shown in Table 1. To mitigate the impact of the external detached shock wave of the probe on the gas flow parameters during the brief 1-3 second test period, a conventional 30° leading edge structure is adopted. The solving model is shown in Figure 2. The aim of this study is to investigate the impact of probe structure on sampling accuracy in supersonic conditions. To achieve this aim, the original basis is extended with a control group of 28° and 32° probes. The computational software FLUENT is utilized for meshing purposes, and the overall grid number is approximately 2 million.

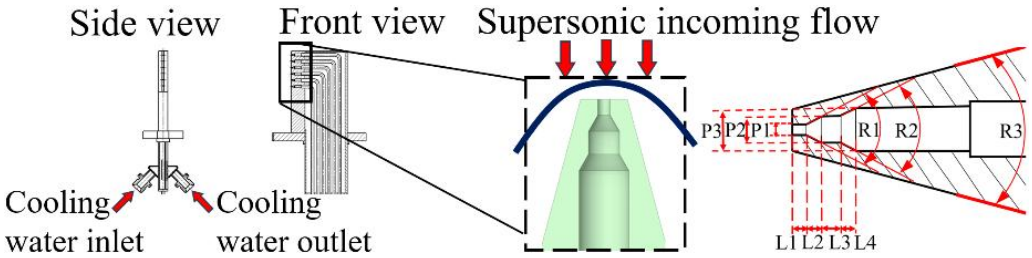

Fig. 1 Structure of the probe

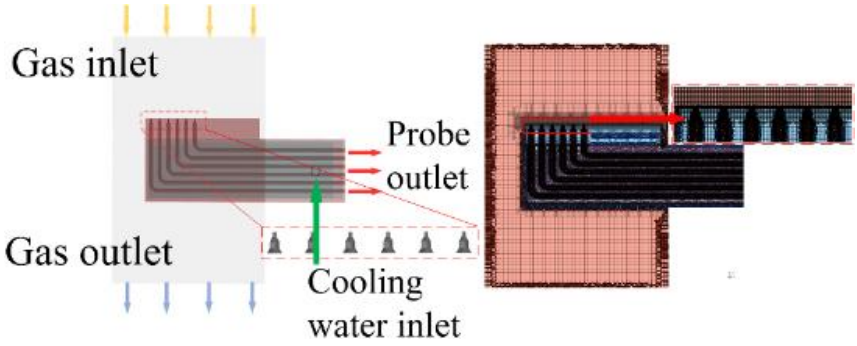

Fig. 2 Solving model

Table 1. Structural parameters of the probe head

Structural parameters	Value
L1/L2/L4	1 mm
L3	1.5 mm
P1	0.8 mm
P2	2 mm
P3	3.2 mm
R1/R2	60±1°
R3	30°

2.2 Numerical calculation methods

The simulation adopts Realizable k-e model of real gas turbulence and combines the computational method of fluid-solid coupling.Five fluid materials, N2, O2, water vapour, CO and CO2, are added to the component transport model and mixed.The specific boundary conditions are shown in Table 2. Since H2 was not detected in the actual test and the content of the remaining UHC was not higher than 0.01%, the influence of CO2 and CO sampling deviation was mainly considered in the simulation calculation.

Table 2. Boundary condition

Boundary	Temperature/K	Pressure/kPa	Initializing gauge pressure /Pa
Gas inlet	2000	2400	48546
Gas outlet	290	102.325	---
Probe outlet	290	75	---
Cold inlet	290	Adjustable	---
Cold outlet	290	101.325	---

The impact of sampling deviation in CO2 volume fraction on combustion efficiency can be assessed using the subsequent equation [11]:

$$\Delta\eta = \frac{\left(0.469\varphi_{CO} + 1.319\varphi_{CH_4}\right)\Delta\varphi_{CO_2}}{\left(\varphi_{CO} + \varphi_{CO_2} + \varphi_{CH_4}\right)^2} \tag{1}$$

The calculation of combustion efficiency in relation to CO sampling bias may be completed using the subsequent equation [11]:

$$\Delta\eta = \frac{\left(0.469\varphi_{CO_2} - 0.85\varphi_{CH_4}\right)\Delta\varphi_{CO}}{\left(\varphi_{CO} + \varphi_{CO_2} + \varphi_{CH_4}\right)^2} \tag{2}$$

The impact of the accuracy of component sampling on overall combustion efficiency can be computed using the subsequent equation [12]:

$$\Delta\delta = \sqrt{\sum_{i=1}^{n}\Delta\delta_i^2} \tag{3}$$

3. Analysis of simulation results of the control groups

3.1 Flow field characteristic analysis

As depicted in Figure 3, a detached shock wave forms in front of the probe, resulting in a drastic and opposing change between the Mach number and static temperature for the probe. This detached shock wave also markedly affects gas flow before the probe entrance at 2-4 mm, causing a sudden decrease in velocity and entry into the subsonic state, coinciding with a sharp increase in static temperature.

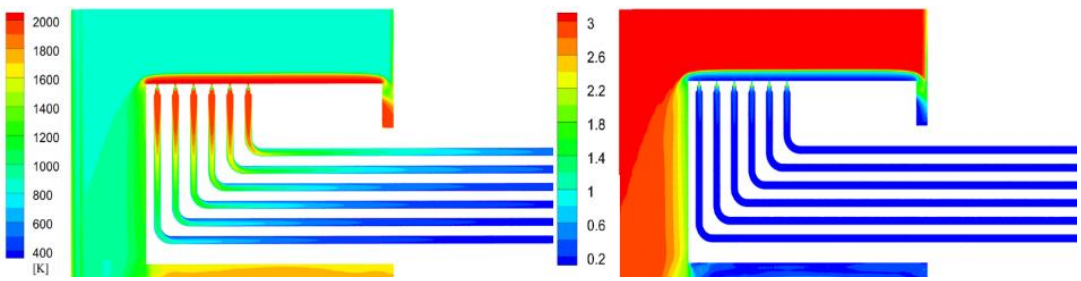

Fig. 3 Distribution of static temperature and Mach number for probe sampling in a supersonic environment

Figure 4 shows the head temperature distribution for the three probe structures. Due to the generation of the detached shock wave, a hemispherical temperature jump zone is formed outside the probe. According to the amplitude of the temperature jumps, it can be initially obtained that the probe with 28° angle has the largest detached distance and the lowest intensity of the shock wave, while the probe with 32° angle has the shortest detached distance and the highest intensity of the shock wave.

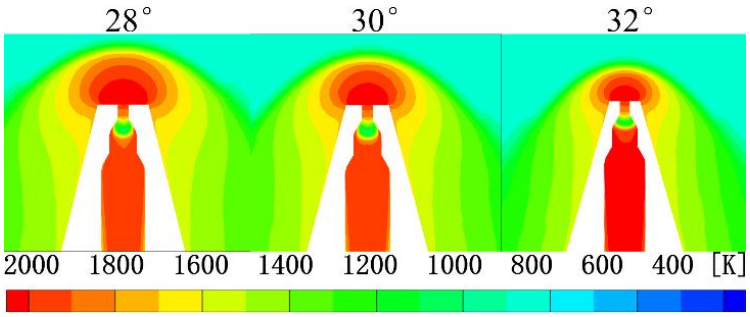

Fig. 4 Distribution of head temperature in different clamping angle probes

Figure 5 gives the change of gas Mach number and static temperature in the probe expansion section as it flows through the inner runner. From the analysis of the figure, it can be seen that in all three structures, the gas flow completes the expansion and compression in the primary expansion section, but the variation of Mach number is small, and the overall expansion and compression effect is poor. This is mainly due to the fact that the gas flow is disturbed by an external detached shock wave, which reduces the Mach number too much and does not fully recover above the speed of sound in the inlet flat section. The 28° and 30° structures freeze better overall, but the 28° structure has less static temperature and Mach number fluctuations.

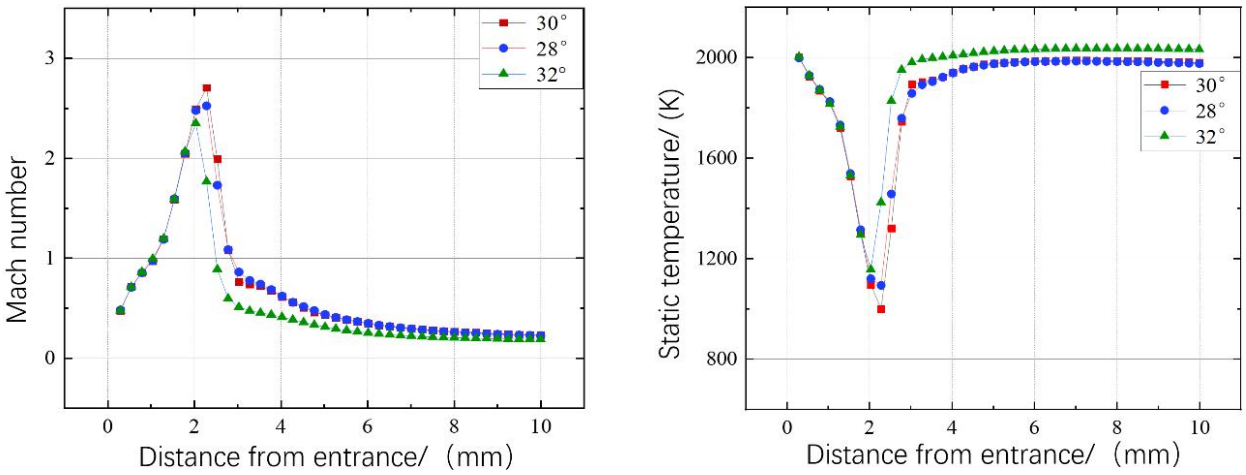

(a) Mach number (b) Static temperature

Fig. 5 Pneumatic parameters of expansion segments with different clamping angle probes

3.2 Component accuracy impact analysis

According to the probe outlet concentration and the ambient molar volume, the relative deviation of the volume fraction of the gas component produced by the probe during operation can be obtained, as shown in Table 3.

Table 3. Relative deviation of volume fractions

Working condition	Water pressure (MPa)	Relative deviation in sampling of CO_2 (%)	Relative deviation in sampling of CO (%)
1	0.5	5.52	5.67
2	0.5	5.31	5.43
3	0.5	5.07	---
4	0.5	5.14	---

From the above table, it can be seen that the relative deviation of CO2 and CO volume fraction produced by working condition 1 is the largest in the actual test. The CO2 and CO contents decrease with an increase in excess air coefficient, which leads to a reduction in volume fraction deviation. Table 4 displays the calculation error of combustion efficiency.

Table 4. Calculation error of combustion efficiency

Working condition	Errors in combustion efficiency due to CO_2 (%)	Errors in combustion efficiency due to CO (%)	Total combustion efficiency error (%)
1	0.201	0.201	0.284
2	0.08046	0.0808	0.114
3	0.007359	---	<0.1
4	0.009663	---	<0.1

Figure 6 shows the correlation between cooling water pressure and relative deviation of gas composition. The gas fraction volume fraction is measured under varying environmental conditions when the cooling water pressure is set at 1- 2 MPa. When the probe clamping angle is set to 30° and 32°, the smallest volume fraction error occurs in condition 1 and condition 2 at 1.75 MPa. The probe's sampling accuracy increases as the cooling water pressure rises with higher CO2 and CO contents. Higher cooling water pressure can improve sampling accuracy for all conditions when the probe angle is 28°. However, the rise rate in sampling accuracy reduces in the range 1.75-2.0 MPa.

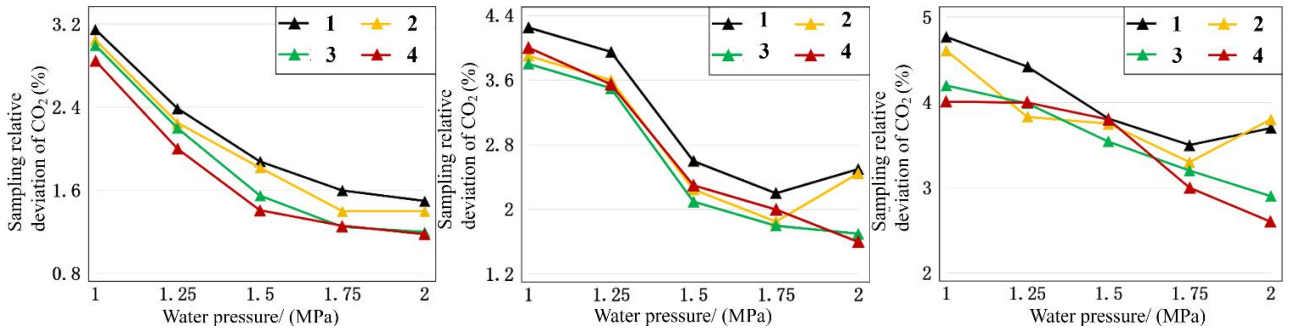

a.28° b.30° c.32°

Fig. 6 Effect of water pressure on CO2 sampling relative deviation

By incorporating the R-K equation, the relative deviation of the volume fraction for CO2 and CO sampling can be computed under optimal sampling conditions at various structures and working conditions. Specific values are presented in Table 5-7.

Table 5. The lowest relative deviation of volume fractions (30°)

Working condition	Optimum water pressure (MPa)	Relative deviation of CO_2 sampling (%)	Relative deviation of CO sampling (%)
1	1.75	2.21	2.27
2	1.75	1.83	1.9
3	2	1.65	---
4	2	1.29	---

Table 6. The lowest relative deviation of volume fractions (28°)

Working condition	Optimum water pressure (MPa)	Relative deviation of CO_2 sampling (%)	Relative deviation of CO sampling (%)
1	2	1.44	1.42
2	1.75-2	1.39	1.36
3	1.75-2	1.21	---
4	2	1.14	---

Table 7. The lowest relative deviation of volume fractions (32°)

Working condition	Optimum water pressure (MPa)	Relative deviation of CO_2 sampling (%)	Relative deviation of CO sampling (%)
1	1.75	3.48	3.4
2	1.75	3.22	3.26
3	2	2.87	---
4	2	2.57	---

It can be seen in the use of the original model and the structure with probe angle larger than 30°, low excess air coefficient is appropriate to use cooling water with pressure about 1.75 MPa. The water pressure needs to be increased when excess air coefficient increases, and CO2 and CO sampling produces the lower deviation in volume fraction. In structures with probe angle 28°, the cooling water pressure can be adjusted between 1.75 and 2 MPa when working in a high excess air coefficient environment, and an inlet pressure of about 2 MPa is appropriate for low excess air coefficient. The table 8-9 displays The lowest calculation error of combustion efficiency from sampling under optimum sampling conditions while using a probe clamp angle of 28° and 32°.

Table 8. The lowest calculation error of combustion efficiency (28°)

Working condition	CO_2-induced errors in combustion efficiency (%)	CO-induced errors in combustion efficiency (%)	Total combustion efficiency error (%)
1	0.05258	0.05015	0.07266
2	0.02110	0.01910	0.02846
3	0.00176	---	<0.01
4	0.002147	---	<0.01

Table 9. The lowest calculation error of combustion efficiency (32°)

Working condition	CO_2-induced errors in combustion efficiency (%)	CO-induced errors in combustion efficiency (%)	Total combustion efficiency error (%)
1	0.1268	0.1204	0.17486
2	0.04884	0.04584	0.06698
3	0.004160	---	<0.01
4	0.004831	---	<0.01

In summary, the 32° probe produces the intensest detached shock wave, resulting in the swift conversion of kinetic energy to thermal energy, and hindering subsequent faster chemical reaction freezing of the structure. Continued increase in the probe angle leads to a further increase in the intensity of the detached shock wave, which produces inferior cooling, and decreasing accuracy.

In contrast, the 28° probe's weaker detached shock wave results in quicker chemical freezing of the structure, which is advantageous to sampling accuracy. Nonetheless, detached distance magnitude somewhat mirrors the chemical reaction's intensity [13]. Of the three angled structures, the probe structure with an angle of 28°produces the greatest detached distance. If the probe angle is decreased further, the detached distance at the front of the probe will increase, leading to an intenser

chemical reaction at the entrance of the probe. Subsequently, the reduction of the probe angle will begin to impact the component accuracy.

4. Optimizing design of the probe structure

4.1 Study of flow field characteristic

In order to further reduce or even circumvent the effect of detached shock wave, the probe head structure is modified to be conical under the premise of ensuring that the probe length remains unchanged. As shown in Figure 7, the meshing and boundary conditions are the same as above. Figure 8 shows the static temperature and Mach number distribution of the modified probe during sampling, and Figure 9 shows the comparison of the velocity distribution of the probe section before and after the modification and marked with flow traces.

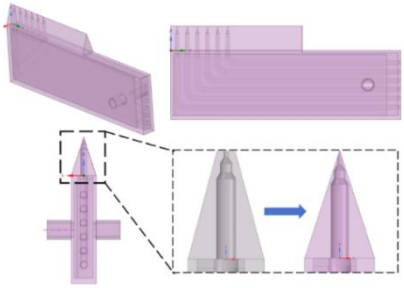

Fig. 7 Modified probe model structure

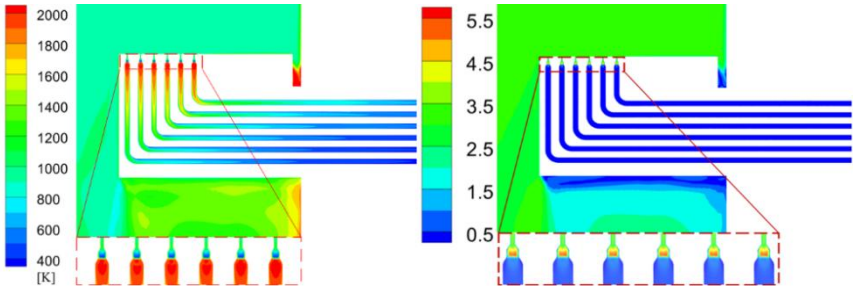

Fig. 8 Static temperature and Mach number distribution

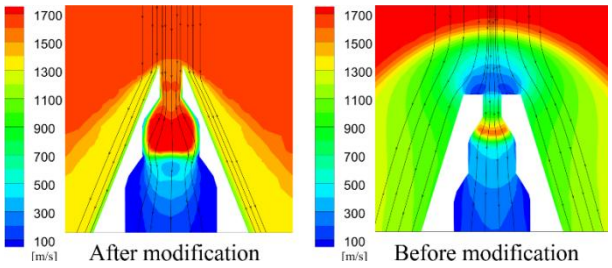

Fig. 9 The gas flow velocity field before and after modification

It can be seen that the front end of the modification probe produces an attached shock wave. The expansion cooling effect of the airflow is significant. The attached shock wave generated outside the modification probe can be approximated as a detached shock wave with the detached distance infinitely close to zero. From the previous section, it can be seen that the very small detached distance further attenuates the chemical reaction, and the sampling accuracy is greatly improved. Figure 10 gives the law of gas static temperature and Mach number of the expansion section of the probe with increasing distance. It can be seen that the gas flow at the front end of the modified probe is smoothly pumped in at a speed close to Mach 3, and when passing through the first expansion wave, the Mach number increases abruptly, and the high-speed gas flow increases the strength of the shock wave dramatically. After compression by the strong shock wave, the gas Mach number falls to subsonic speed in a short time and the static temperature value can be as low as about 400 K, with an excellent expansion cooling effect.

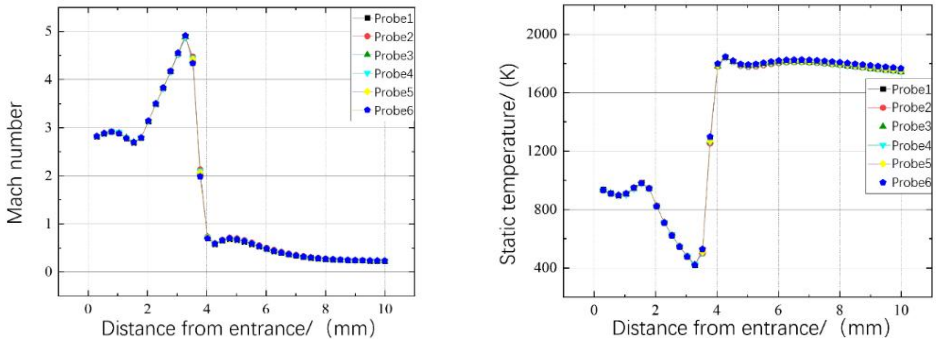

a. Mach number b. Static temperature

Fig. 10 Mach number and Static temperature of gas in the expansion section

4.2 Component accuracy impact analysis

Figure 11 shows the variation of CO2 sampling relative deviation of the modified probe under different working conditions and different cooling water pressure. It can be seen that the sampling accuracy increases with the increase of water pressure in the four working conditions, and the accuracy improvement decreases under 1.5-2.0 MPa water pressure.

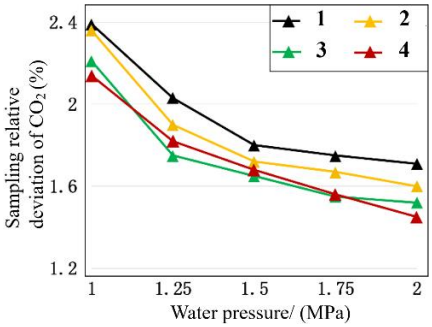

Fig.11 Impact of cooling water pressure on CO2 sampling error

The tables 10-11 demonstrate the relative deviation of volume fractions produced by sampling under test conditions and the lowest relative deviation in volume fractions. It is clear that the relative deviation of the volume fraction obtained from the modified probe is lower than that from the original structure, regardless of whether the working water pressure of 0.5 MPa or the optimum inlet pressure is used.

Table 10. Relative deviation of volume fractions (modified probe)

Working condition	Water pressure (MPa)	Relative deviation of CO_2 sampling (%)	Relative deviation of CO sampling (%)
1	0.5	4.25	3.31
2	0.5	4.18	3.26
3	0.5	3.97	---
4	0.5	4	---

Table 11. The lowest relative deviation of volume fractions (modified probe)

Working condition	Optimum water pressure (MPa)	Relative deviation of CO_2 sampling (%)	Relative deviation of CO sampling (%)
1	2	1.7	1.61
2	2	1.57	1.63
3	2	1.43	---
4	2	1.43	---

The Tables 12-13 present the calculation error of combustion efficiency from the modified probe under test and optimal sampling conditions. It can be concluded that the calculation error of combustion efficiency of the modified probe is significantly reduced.

Table 12. Calculation error of combustion efficiency (modified probe)

Working condition	CO_2-induced errors in combustion efficiency (%)	CO-induced errors in combustion efficiency (%)	Total combustion efficiency error (%)
1	0.1547	0.117	0.194
2	0.06331	0.04584	0.07816
3	0.005759	---	<0.01
4	0.007516	---	<0.01

Table 13. The lowest calculation error of combustion efficiency (modified probe)

Working condition	CO_2-induced errors in combustion efficiency (%)	CO-induced errors in combustion efficiency (%)	Total combustion efficiency error (%)
1	0.06186	0.05684	0.084
2	0.02374	0.02294	0.033
3	0.002080	---	<0.01
4	0.002684	---	<0.01

4.3 Comparative analysis before and after structural modification

Figure 12 displays the comparison of the gas Mach number and static temperature change law before and after modifying the probe structure in the supersonic environment.

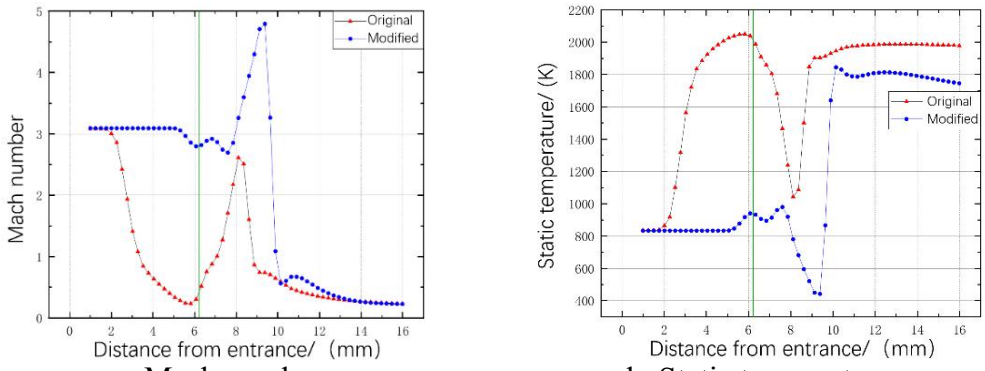

a. Mach number b. Static temperature

Fig.12 Change in Mach number and static temperature of gas before and after modification

From the analysis of the figure, it can be seen that the gas enters the probe only once to produce expansion and compression, but the gas expansion of the modified probe is more complete, and the chemical reaction freezing effect is better. The gas enters the modified probe at the instant of the gas flow Mach number is higher, the intensity of the expansion wave and the shock wave generated at the first expansion channel is larger. Both structures are compressed before the expansion section, and the gas velocity can be reduced to subsonic and below, but the overall static temperature of the modified probe is lower. At high Mach numbers, the resistance of the shock wave accounts for an extremely high percentage of the total resistance. At the same time, the high temperature environment makes the probe more prone to ablation, and the detached shock wave is very unfavorable to the freezing of chemical reactions in the gas flow, in addition to the drastic changes in the gas flow parameters. The above comparative analysis shows that the modified probe is more suitable for supersonic sampling environments.

5. Experimental verifications

Figure 13 shows a single head combustion chamber test bench. A total of five trials are set up to research the sampling laws of gas. During the test, the cooling water pressure is set at 0.5 MPa. At the probe outlet, several sets of temperature and pressure sensor measurement points are arranged.

Fig.13 Single head combustion chamber test bench

Table 12 records the parameters of the concentration of each component of the combustion chamber outlet gas at different excess air coefficient, where T represents the temperature of the outlet measurement point of the mixed gas sample. When the excess air coefficient is low, there is an increase in the percentage of CO2 and due to incomplete combustion, the concentrations of CO and NO pollutants increase. Following screening, the preferred excess air coefficient is selected for simulation analysis and comparative validation, within the range of 1.14-2.06.

Table 12. Concentration data of gas components of a test platform

excess air coefficient (Alf)	HUC (ppm)	CO_2(%)	CO (ppm)	NO (ppm)	NO_2(ppm)	NOx(ppm)	T(K)
2.06	75.11	7.03	283.66	53.72	12.09	67.15	572.84
1.61	45.40	9.07	407.93	82.60	18.58	103.25	577.12
1.25	43.90	11.52	3685.24	130.26	29.31	162.83	586.47
1.14	97.51	11.79	10611.91	130.71	29.41	163.39	587.35

The results show that the total error between the test results and the simulation data is not more than 5%, and the results are considered reliable considering the possible existence of chemical reactions.

6. Summary

On the basis of the original structure, reducing the Angle of air intake to 28° can improve the component accuracy of sampling in supersonic gas to a certain extent, but cannot avoid the impact of detached shock wave on the sampling accuracy. The modified probe effectively avoids the effect of detached shock wave and the sampling accuracy is greatly improved. In the original structure, when the excess air coefficient is 1.14, the maximum error of total combustion efficiency is 0.284%. The total combustion efficiency error of the modified probe is 0.084%, which is a decrease of 70.42%.

References

[1] Shan X M, Gao Q and Wei X L. Test and Measurement Technology for Aero Engines. Aerospace Power 2022; 26(03): 67-70.

[2] Ju H Y, Liang H X, Suo J Q, et al. Pollution emission characteristics of hydrogen-fueled combustor of an aero-engine conversion gas turbine. Journal of Propulsion Technology Epub ahead of print 9 January 2024. DOI: 10.13675/j.cnki.tjjs.2209039.

[3] Qiao Q B, Fang C Y, Mu Y, et al. Numerical Analysis and Experiment Research on Flow Field of a Micro-gas Turbine Combustor. Gas Turbine Technology 2021; 34(03): 28-32+62.

[4] Qing S, Application of a thermocouple to the measurement of the temperature field at the exit of a combustion chamber. Electronic Production 2019; 19: 68-70.

[5] S Williamson R and Stanforth C. Measurement of Jet Engine Combustion Temperature by the Use of Thermocouples and Gas Analysis. SAE paper 1969-690433, 1969.

[6] Bideau R J. The Development of a Computer Code for the Estimation of Combustor Exhaust Temperature Using Simple Gas Analysis Measurements. J Eng Gas Turbine Power 1999; 121(1): 80–88.

[7] Sevcenco, YA, Crayford, AP, Marsh, R, et al. Evaluation of a Particulate Sampling Methodology From a Gas Turbine Exhaust Using Real-Time Size and Number Analysis at Simulated Aircraft Conditions. Turbo Expo: Power for Land, Sea, and Air 2010; 43970: 1113-1124.

[8] Mutschler R, Luo W, Moioli E, et al; Fast real time and quantitative gas analysis method for the investigation of the CO2 reduction reaction mechanism. Rev. Sci. Instrum. 2018; 89(11): 114102.

[9] ISO ARP1256D:2011. Procedure of the continuous sampling and measurement of gaseous emissions from aircraft turbine engines.

[10] ISO ARP1533C:2016. Procedure for the analysis and evaluation of gaseous emissions from aircraft engines.

[11] Wang M R, Xiao Y, Han B, et al. Gas analysis test and calculation method of aeroengine. Journal of Aerospace Power 2015; 30(11): 2568-2574.

[12] Li Y J, Wang M R, Han B, et al. Gas turbine primary combustor error analysis of combustion efficiency and exhaust emission using gas analysis method. Journal of Aerospace Power 2017; 32(5): 1051-1057.

[13] Liao D J, Liu S, Jian H X, et al. Review of research on shock standoff distance for hypersonic sphere. Journal of Experiments in Fluid Mechanics 2015; 29(6): 1-8,27.